Geomechanics and Engineering, *Vol. 6, No. 5 (2014) 487-502*
DOI: http://dx.doi.org/10.12989/gae.2014.6.5.487

Numerical modeling of rapid impact compaction in loose sands

Elham Ghanbari [a] and Amir Hamidi [*]

Department of Engineering, Kharazmi University, Tehran, Iran

(*Received August 10, 2013, Revised January 02, 2014, Accepted January 07, 2014*)

Abstract. A three dimensional finite element model was used to simulate rapid impact compaction (RIC) in loose granular soils using ABAQUS software for one impact point. The behavior of soil under impact loading was expressed using a cap-plasticity model. Numerical modeling was done for a site in Assalouyeh petrochemical complex in southern Iran to verify the results. In-situ settlements per blow were compared to those in the numerical model. Measurements of improvement by depth were obtained from the in-situ standard penetration, plate loading, and large density tests and were compared with the numerical model results. Contours of the equal relative density clearly showed the efficiency of RIC laterally and at depth. Plastic volumetric strains below the anvil and the effect of RIC set indicated that a set of 10 mm can be considered to be a threshold value for soil improvement using this method. The results showed that RIC strongly improved the soil up to 2 m in depth and commonly influenced the soil up to depths of 4 m.

Keywords: rapid impact compaction; numerical modeling; cap plasticity; set; relative density

1. Introduction

Rapid impact compaction (RIC) is an alternative method for over-excavation and replacement when improvement at depths of more than 2 m is desired (Becker 2011). This method was first used in the UK in the early 1990s to modify bomb craters in airfield runways (Watts and Charles 1993, Allen 1996, Serridge and Synac 2006). A RIC is installed on a hydraulic excavator and is composed of a hammer (7 to 12 t), a 1.5 m diameter anvil made of steel, and a data acquisition system that records soil settlement per blow, total depth, and energy during operation. Soil compaction is obtained by producing impact energy via hammer free fall from a height of 1.0 to 1.5 m onto the anvil, which remains on the soil during compaction. The anvil transfers energy to the soil and turns it into compaction energy. The blows are very fast, with a time length of 1.2 to 1.5 s and a speed of 40 to 50 blows per min.

Most studies on RIC have been field investigations. Watts and Charles (1993) measured the degree and depth of compaction over several trials. Other field studies were performed by Allen (1996), Kristiansen and Davies (2004), Tara and Wilson (2004), Serridge and Synac (2006), Simpson *et al*. (2008), Becker (2011), and Vukadin (2013). Physical modeling of RIC has also been done in the laboratory using centrifuge testing (Merrifield *et al*. 1998, Parvizi 1999, Merrifield and Davies 2000, Parvizi and Merrifield 2000, Parvizi 2006, Parvizi 2009). Recently,

*Corresponding author, Associate Professor, E-mail: hamidi@khu.ac.ir
[a] Graduate Student

http://www.techno-press.org/?journal=gae&subpage=7 ISSN: 2005-307X (Print), 2092-6219 (Online)

numerical studies have been performed to evaluate RIC (Falkner *et al*. 2010, Adam *et al*. 2011).

RIC is similar to deep dynamic compaction (DDC). In both methods, compaction energy produced by impact dissipates by plastic deformation and viscous damping. Plastic deformation produced in the soil media results in compaction of the soil (Ghassemi *et al*. 2009, Falkner *et al*. 2010). More numerical studies exist on DDC (Pan and Selby 2002, Lee and Gu 2004, Ghassemi *et al*. 2009, Jia and Zhou 2010), probably because of the higher speed of operation, shorter time interval between impacts, and more impact blows (up to 99 blows) required to complete compaction, which is difficult for numerical simulation. As a result, there are a number of unknowns, such as the depth of improvement per blow and the relation between settlement and blow count. The present study investigated the compaction mechanism in RIC and the effects of different parameters on efficiency.

2. Site specifications and soil parameters

Soil characteristics and RIC parameters for the Assalouyeh petrochemical complex site located in southern Iran were used in the model (Yasrebi and Asghari 2004). The soil type is non-plastic silty gravel with sand (GM) and a passing percentage of 18.4% for a no. 200 sieve (0.075 mm). Representative soil gradation is shown in Fig. 1. A trial backfill 5 m in depth was built on site to investigate improvement by depth using RIC. The in situ tests were performed before and after compaction were the standard penetration test (ASTM D1586), plate load test (ASTM D1195), and large density test (ASTM D5030). SPT results before and after compaction are shown in Fig. 2. The water table was below 20 m and the soil was dry (SPI Co. 2006).

Before compaction, the elastic modulus varied from 60 to 150 kg/cm^2 by depth. It increased to 470 kg/cm^2 as measured by the after-compaction plate load test. Soil densities before and after compaction at different depths was measured using the large density test and are shown in Table 1 (SPI Co. 2006).

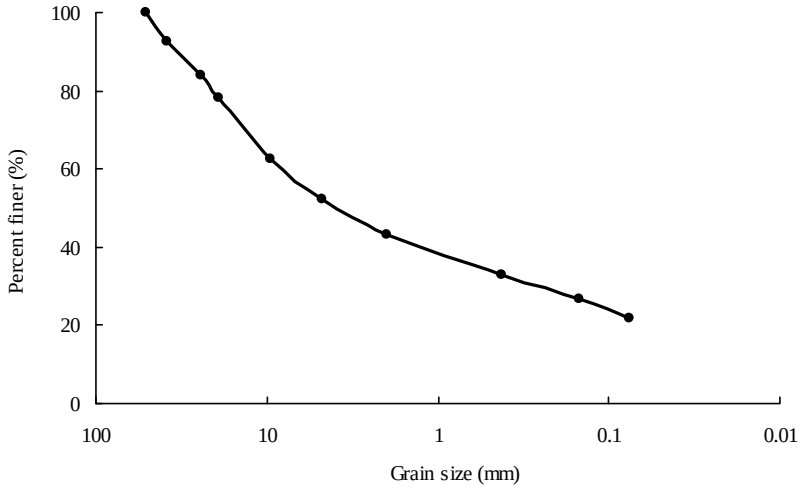

Fig. 1 Representative gradation of soil in Assalouyeh site

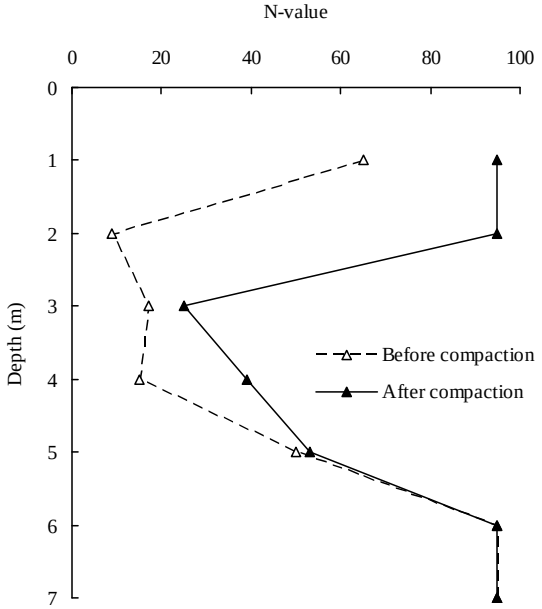

Fig. 2 Variation of before and after compaction SPT N-values in trial backfill

Table 1 Before and after compaction soil density in trial backfill

Depth (m)	Before compaction density (gr/cm^3)	After compaction density (gr/cm^3)
0.0	1.75	2.18
2.0	1.78	2.21
4.0	1.77	2.09

3. Numerical model

Several factors should be considered for numerical modeling of RIC, including simulation of impact loads, dynamic analysis, damping parameters, a constitutive model, interface element types, and dimensions of the model. ABAQUS finite element software considers all these parameters and was used in this study.

3.1 Geometry of the model

The dimensions of the model were selected to be 7 × 7 m after trial and error showed that the density of energy, velocity, and acceleration of particles at the boundaries were low enough to prevent wave reversal effects. The hammer and anvil were made of steel with a density of 7800 kg/m^3. The hammer was modeled as cylindrical in shape with a weight of 9.0 t. The anvil was modeled as a cone with a 1.5 m diameter at the bottom and 1.0 m diameter at the top. The falling height was 1.1 m both on site and for the model. The numerical model and RIC components are shown in Figs. 3 and 4, respectively.

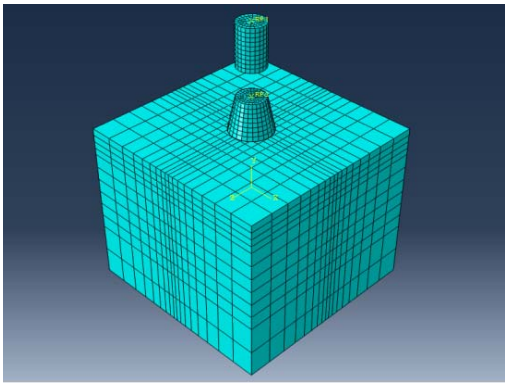

Fig. 3 Numerical model and finite element mesh

Fig. 4 RIC device components

Fig. 3 also shows the finite element mesh used in the model. Hexahedral elements were used as the soil, hammer, and anvil to give a regular shape to the model. To achieve more accurate results in the analysis, a finer mesh size was considered in the vicinity of the anvil where the concentration of stress was higher. The mesh size under the anvil was about 0.15 m at the surface and 0.25 m at depth. At the boundaries, it was 0.8 m on the surface and 1.0 m at depth.

3.2 Simulation of impact loads

A number of researchers have presented time histories for stress or acceleration of impact loads (Scott and Pearce 1975, Mayne and Jones 1983, Roesset *et al*. 1994). Pan and Selby (2002) proposed two methods for applying impact loads. The first is to determine the applied load time history by multiplying the mass of the hammer by the acceleration time history as a damped half-sine wave. The second method is simulation of the contact of a rigid body by application of the impact velocity to the ground surface.

A third method was used in the present study. The hammer is modeled as a rigid body that falls from a specified height and gravity loads are applied to the nodes. After a specific time, it returns

to its initial location and the second impact is applied. The initial velocity is applied at the ground surface and the elastic strains are removed at the beginning of the unloading step.

3.3 Damping parameters

Rayleigh damping parameters were used to consider viscous damping based on Eq. (1), where α and β are the constants of vibrating mass and stiffness, respectively, which are proportional to the frequency of loading.

$$C = \alpha M + \beta K \tag{1}$$

Here, C is the damping matrix, M is the vibrating mass matrix, and K is the stiffness matrix of the system. For impact problems, higher mode frequencies affect the damping matrix if α is considered to be zero. β can be calculated based on the following equation (Bathe 1996)

$$\beta = \frac{2\mathrm{D}\omega}{\omega_1 + \omega_n} \tag{2}$$

D is the damping ratio and is considered to be 5%, ω_1 is the minimum frequency (0.01 Hz) and ω_n is the maximum frequency (100 Hz) (Rix *et al*. 2000). Natural frequency ω is assumed to be 10 Hz (Pan and Selby 2002). Geometric damping was assumed when the model dimensions were created.

Contact interaction was used between anvil and hammer to consider proper interaction between the two surfaces. This type of interaction considers tangential and normal forces. For tangential forces, penalty friction formulation was used to apply frictional forces using a frictional coefficient of 0.5. For normal forces, hard contact property was used where the total compressive stresses are transferred through the bodies during the contact period. The interaction between the anvil and the ground surface was the same; however, they were not allowed to separate during contact.

Implicit direct integration was used, which is more appropriate for this type of analysis (Sun *et al*. 2000). A minimum time increment for dynamic analysis is 10^{-8} s and the time period for each impact is 1.5 s (40 blows per min). The large displacement option is used to consider geometrical nonlinearity during analysis.

3.4 Constitutive law

Although the behavior of soil under impact loads cannot be predicted by an elastic model, previous studies have considered the soil beneath the tamper to be an elastic column (Chow *et al*. 1990). Other numerical studies on dynamic compaction have assumed elasto-plastic behavior for the soil (Scott and Pearce 1975). Pan and Selby (2002) used the Mohr-Coulomb model to simulate soil behavior during dynamic compaction. Adam *et al*. (2011) modeled the soil as an elasto-plastic half-space based on Mohr-Coulomb theory. Most of these models could not predict soil failure under compression (Ghassemi *et al*. 2009). The Mohr-Coulomb model assumes that failure takes place under shear stress, while major plastic volumetric strain and yield result from high compressive stress under impact. This aspect of behavior can be easily predicted using the cap-plasticity model used to simulate behavior under impact loading (Lee and Gu 2004, Pak *et al*. 2005, Ghassemi *et al*. 2009).

Modern cap-plasticity models were first introduced by Dimaggio and Sandler (1971). In their

study, the yield surface consisted of a shear failure envelope, moving cap and tension cut-off. The shear failure envelope consisted of two shear yield surfaces, the Drucker-Prager envelope at the beginning that connected smoothly to the von Mises envelope. Poran and Rodriguez (1992) proposed a single shear yield surface to predict soil behavior in dynamic compaction analysis.

The cap-plasticity model in ABAQUS consists of two parts. The first, f_1, is a linear shear yield surface based on the Drucker-Prager criterion in Eq. (3) that is fixed and defined in the first and second stress invariant planes (J_1, $\sqrt{J_{2D}}$). In this equation, θ and κ are constants of the Drucker-Prager failure criterion and can be determined using friction angle φ and cohesion intercept c, based on Eqs. (4) and (5). The second yield surface, f_2, is a moving cap defined by Eq. (6) and used to express yield and plastic volumetric strains under effective isotropic stress. R is the material parameter and l is the first invariant of the stress tensor at the intersection of the fixed yield surface and moving cap. It can be calculated based on hardening parameter X in each step according to Eq. (7). The cap is extended because of the hardening rule for the plastic volumetric strain ($d\varepsilon_v^p$) in each step and is defined by Eq. (8).

$$f_1 = \sqrt{J_{2D}} - \theta J_1 - \kappa \tag{3}$$

$$\alpha = \frac{2\sin\varphi}{\sqrt{3}(3-\sin\varphi)} \tag{4}$$

$$\kappa = \frac{6c\cos\varphi}{\sqrt{3}(3-\sin\varphi)} \tag{5}$$

$$f_2 = (J_1 - 1)^2 + R^2 J_{2D} - (X - l)^2 \tag{6}$$

$$l = \frac{X - \kappa R}{1 + \theta R} \tag{7}$$

$$X = -\frac{1}{D} Ln(1 - \frac{\varepsilon_V^p}{W}) + X_0 \tag{8}$$

Here, W and D are material parameters and X_0 is the mean effective stress according to gravity analysis. It has different values at different soil depths (h) and is calculated based on the unit weight of the soil (γ) and the at-rest earth pressure coefficient (k_0) in Eq. (9)

$$X_0 = \frac{\gamma h(1 + 2k_0)}{3} \tag{9}$$

Fig. 5 Shows the cap-plasticity yield surfaces in the $J_1 - \sqrt{J_{2D}}$ plane. The cap-plasticity parameters were determined based on the soil characteristics for the Assalouyeh site. W, R and D were selected based on values suggested by Oshima and Takada (1997), Lee and Gu (2004) and Ghassemi *et al*. (2009) and are shown in Table 2.

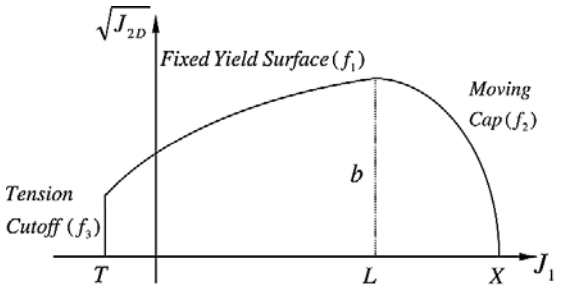

Fig. 5 Yield surface of cap-plasticity model

Table 2 Soil and cap plasticity model parameters

Cap plasticity model parameters			Drucker-Prager constants		Soil characteristics for Assalouyeh site	
W	D (m^2/kN)	R	θ	κ	c (kN/m^2)	φ (degree)
0.4	0.00018	4.33	0.19	0.0	0.0	25

4. Verification of the model

RIC automatically records information during the compaction process. The number of blows, settlement of soil per blow, total penetration depth of the anvil, and total input energy are recorded. Settlement under the anvil per blow is the "set" and its value in the last blow is the "final set". Crater depth is the total set from the first blow to the last.

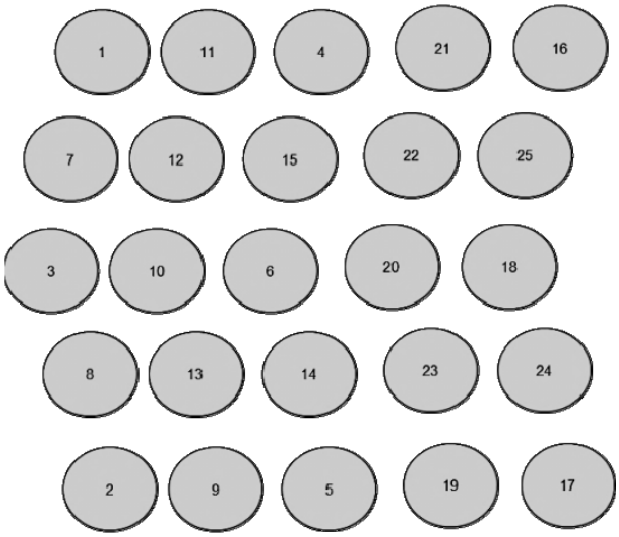

Fig. 6 Pattern of compaction for 25 points

RIC was applied at 25 compaction points for the trial backfill considered in this study. Fig. 6 shows the pattern of compaction for 25 points in the site. If the soil met one of the following conditions, compaction at that point automatically ceased

(1) Crater depth is more than 900 mm
(2) Final set reaches 2 mm
(3) The number of blows is greater than 99
(4) Problems are encountered during compaction, such as facing cobbles under the anvil

Where no mutual interaction occurred between compaction points, a single point was selected for verification of the numerical model. In situ settlement values per blow were compared to the numerical results. Fig. 7 shows a comparison of settlements per low recorded from the device for two points with the numerical model results. Settlement in the first blow was 48.6 mm for numerical analysis and 52 mm and 61 mm for the two compaction points. In the 10^{th} blow, it decreased to 18 and 19 mm for the points and 18.3 mm for the numerical analysis. The final set for the field compaction points were 4 mm and 5 mm for 75^{th} and 78^{th} blows for final crater depths of 878 mm and 860 mm, respectively. For the numerical model, the final crater depth was 901 mm (more than 900 mm) in the 80^{th} blow.

There was fairly good agreement between the numerical results and field data. Settlement values decreased for both numerical and field results; however, the trend increased for some blows in the numerical analysis. For instance, for the 41^{th} blow, the set was 9.1 mm and for the 42^{th} blow, the set was 10.1 mm. In the numerical analysis, soil parameters such as elastic modulus and density were not upgraded as the relative density increased for each blow, probably as a result of a kink in the numerical analysis results compared to the field data.

In Eq. (10), P_b is the ratio of the blow count (N) of a specified set to total blows (N_t). P_d is the ratio of crater depth (Z) at blow count N to a specified set of total crater depth (Z_t). The specified set is between 1 and 10 mm. N and Z were chosen when the first specified set was obtained.

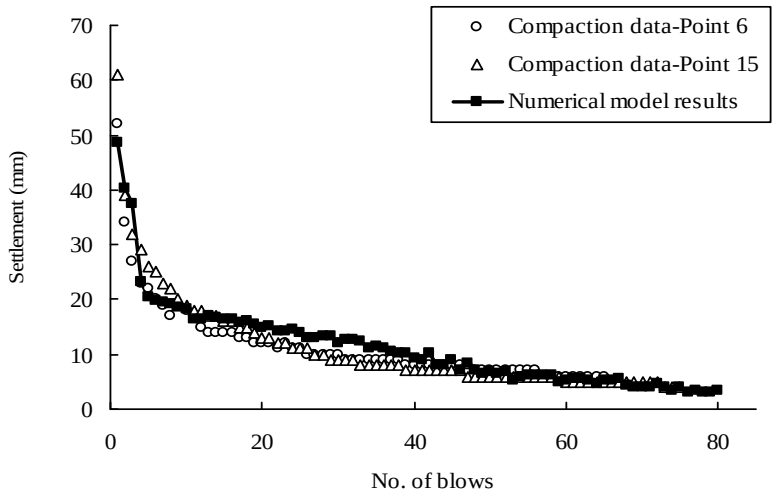

Fig. 7 Comparison of the settlement per blow count for numerical model and field data

$$P_b = \frac{N}{N_t} \times 100 \tag{10}$$

$$P_d = \frac{Z}{Z_t} \times 100 \tag{11}$$

Fig. 8 depicts the variation in P_d versus P_b for numerical analysis; all compaction points showed good consistency.

Plastic volumetric strain (ε_v^p) can also be determined for each node by numerical analysis. The after-compaction void ratio and dry unit weight based on this value were calculated using Eqs. (12) and (13)

$$e_1 = e_0 - (1 + e_0)\varepsilon_v^p \tag{12}$$

$$\gamma_d = \frac{G_s \gamma_w}{1 + e_1} \tag{13}$$

where e_0 is the initial void ratio, e_1 is the after-compaction void ratio, ε_v^p is the plastic volumetric strain produced during compaction, G_s is the specific density of the soil solids, γ_d is the dry density of the soil and γ_w is the density of the water. Table 3 compares the after-compaction unit weights recorded by in situ large density tests and values calculated using numerical analysis. It resulted in a difference of less than 10% between the numerical results and the in situ test data.

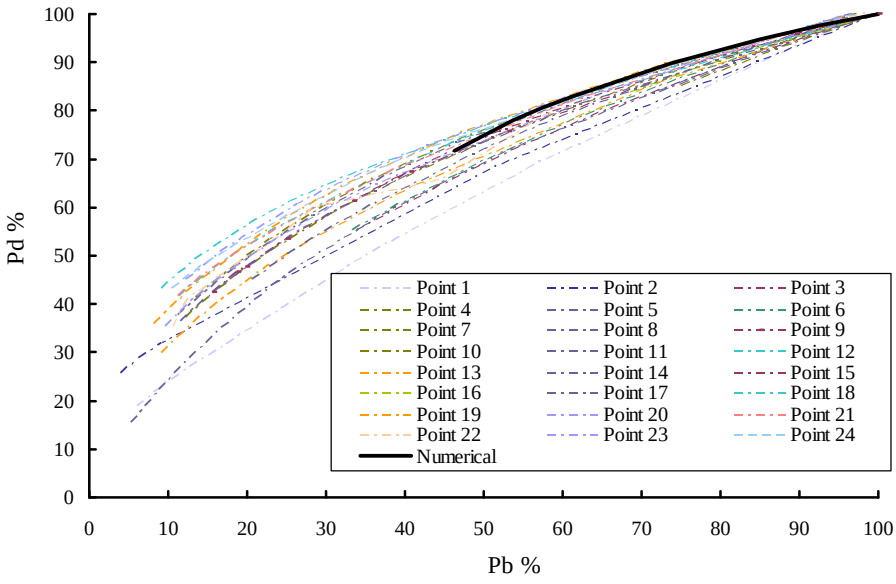

Fig. 8 Percent of crater depth versus percent of blows for numerical analysis and field data

Table 3 After compaction dry unit weights recorded from large density tests and numerical analysis

Depth (m)	In site unit weights (gr/cm^3)	Numerical unit weights (gr/cm^3)
0.00	2.18	2.37
2.00	2.21	2.33
4.00	2.09	1.88

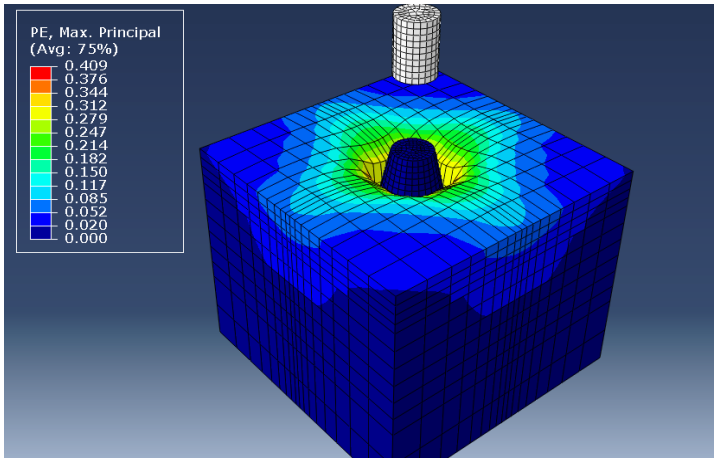

Fig. 9 Top view of plastic volumetric strain contours

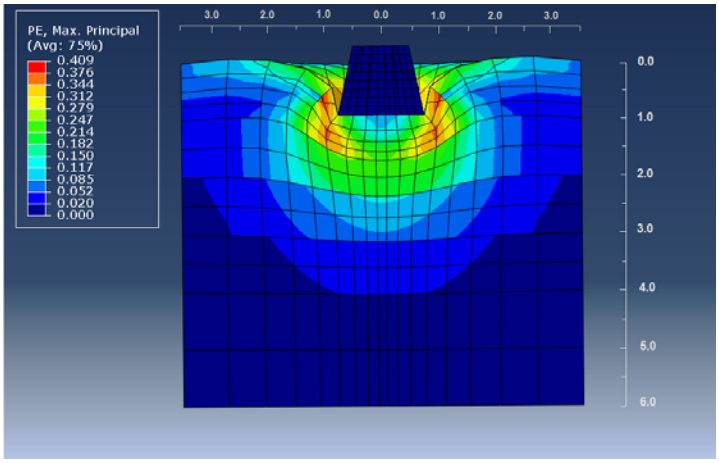

Fig. 10 Side view of plastic volumetric strain contours

5. Results of numerical analysis

Figs. 9 and 10 show the top and side views of the plastic volumetric strain contours determined from the numerical model. It can be seen that the maximum strain level was 0.4 at the ground

surface. The minimum calculated strain from the model was 0.02 at a depth of 4 m below the anvil. Plastic volumetric strain decreased to zero at greater depths, which shows the lack of influence of compaction for the soil using the 9 t hammer and 1.1 m drop height and indicates that the soil was affected up to 4 m in depth. Lateral extension was about 3.5 m from the center of the anvil between the ground surface and 0.5 m in depth and 1.9 m between 0.5 m and 4 m in depth. It can be concluded that little mutual interaction occurred between adjacent compaction points, except near the surface (up to 0.5 m in depth).

Fig. 11 shows the after-compaction relative density contours obtained by numerical analysis. It can be observed that a stiff soil plug with over 100% relative density formed immediately below the impact point and developed to up to 2 m in depth (zone 1). This phenomenon was also reported by Becker (2011). Fig. 11 shows that lateral deformation at the ground surface was about 1.7 m from the center of the impact area. After that, zone 2 developed with a relative density of 75% to 100% between 2.0 to 2.7 m in depth and was classified as very dense soil. It also developed laterally up to 2.5 m from the center. Zone 3 had a relative density of 50% to 75% at 2.7 to 3.2 m

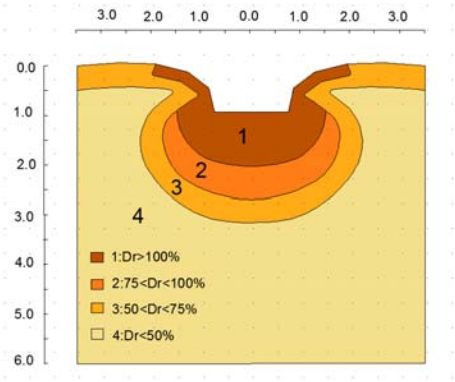

Fig. 11 Contours of equal relative density

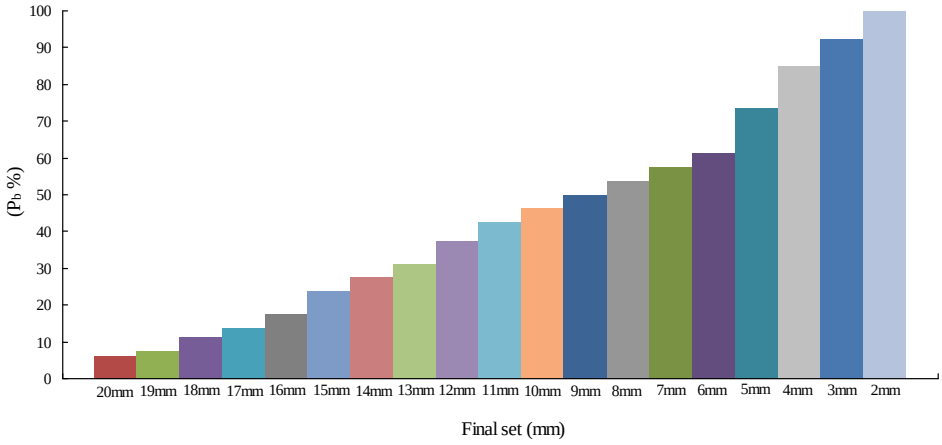

Fig. 12 Variation of P_b with desired final set

in depth and was classified as medium-compacted soil. It extended in the lateral direction up to 3.5 m from the center. Zone 4 occurred below 3.2 m in depth and was not influenced by RIC.

Fig. 12 shows the percentage of blows (P_b) required to reach the desired final set of 20 to 2 mm. As observed, 46% of total blows were required to reach the final set of 10mm and 54% more blows were needed to reach the final set from 10 to 2 mm. It is important to investigate the relation between the degree of soil improvement and the desired final set. Consideration of the relation between final set and degree of improvement is also useful to determine the optimum number of blows.

Fig. 13 shows the variation in average relative density between 0 to 1 m in depth by the number of blows. Initial relative density was 26%, which increased to 100% by the 50th blow. Table 4 is based on the data from Fig. 13 and represents data for the variation in average relative density between 0 to 1 m in depth by the number of blows. As indicated, the relative density reached about 100% by the application of 60% of the total blows.

Fig. 14(a) shows the variation of average relative density at 0 to 1 m in depth with a final set of 10 to 3 mm. A set value of 10 mm produced a relative density of 90% at this depth. It can be concluded that a set of 10 mm was adequate to reach the desired soil improvement up to 1 m in depth. Lower set values only led to the application of unnecessary blows, wasting energy.

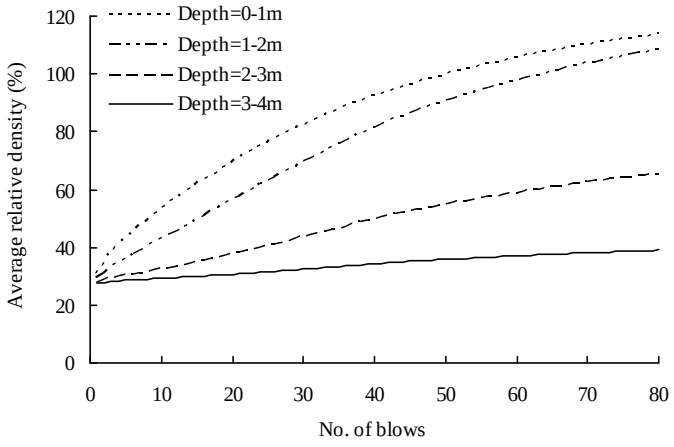

Fig. 13 Variation of the average relative density with blow count

Table 4 Variation of the average relative density with percent of applied blows

Blow count	(N/N_t)%	Dr% (0.0~1.0 m)	Dr% (1.0~2.0 m)	Dr% (2.0~3.0 m)
40	50	92.4	81.4	49.6
48	60	98.4	89.1	53.8
56	70	103.5	95.0	57.3
64	80	107.6	100.2	60.3
72	90	111.0	104.7	63.1
80	100	113.7	108.4	65.4

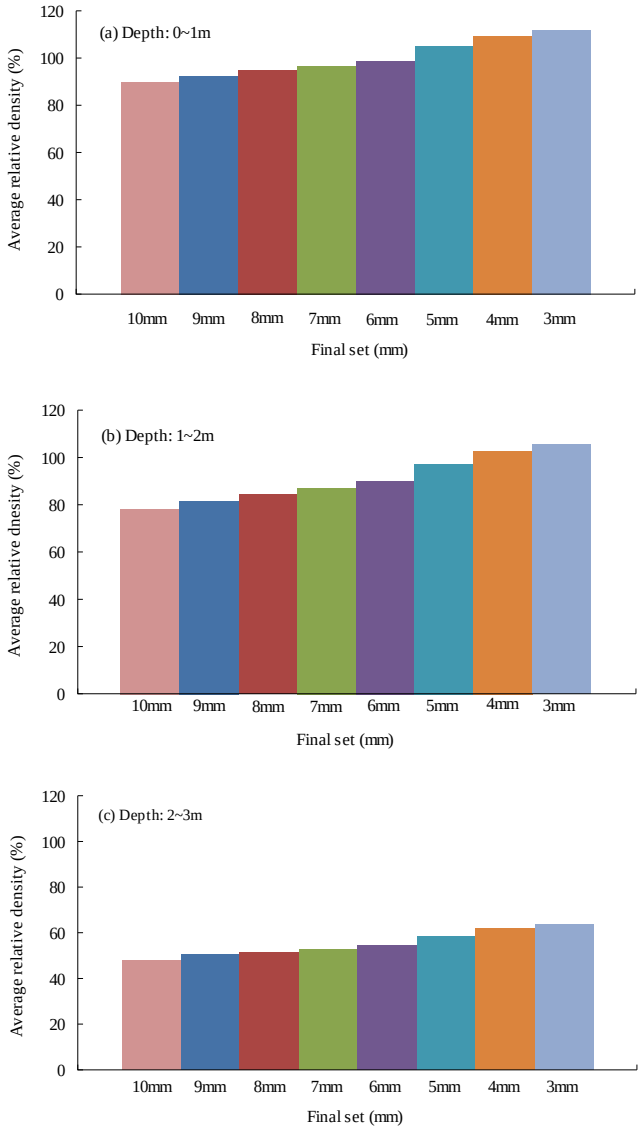

Fig. 14 Variation of relative density with final set

Fig. 13 shows that the variation in average relative density at 1 to 2 m in depth by the number of blows. The soil reached 100% relative density at the 64th blow. Further compaction took place at this depth until the 80th blow. Table 4 shows the data for the variation in average relative density from 1 to 2 m depth by percentage of blows. As shown, the soil reached 100% relative density at 1 to 2 m in depth by the application of 80% of total blows.

Fig. 14(b) shows the variation in relative density at 1 to 2 m in depth with a final set of 10 to 3 mm. The relative density reached 78.2% in the final set at 10 mm, which shows an appropriate degree of improvement at this depth.

The variation of average relative density at 2 to 3 m in depth by the number of blows is also depicted in Fig. 13. As seen, the soil never reached 100% relative density at this range of depth. The maximum relative density was 65.3% at the 80th blow and the rate of improvement by blow count was less than at lower depths. Table 4 shows the data for the variation in relative density at 2 to 3 m in depth by percentage of blows. Comparing the data in columns 3 and 4 of Table 4 reveals that the soil reached a relative density of 60.3% at the 64th blow (relative density = 107.6% at 0 to 1 m in depth and 100.2% at 1 to 2 m in depth).

Fig. 14(c) shows the variation in relative density at 2 to 3 m in depth with a final set of 10 to 3 mm. It can be seen that the relative density increased from 48% to 63.7% when the final set decreased from 10 to 3 mm, which is in the medium compaction range, compared to lower depths.

Fig. 13 represents the variation in average relative density at 3 to 4 m in depth by blows. It can be observed that the soil reached a relative density of 40% at the 80th blow at this depth. It is clear that the rate of improvement was extremely small compared that at lower depths and the soil was only slightly affected by a further increase in the number of blows.

6. Conclusions

- The present study numerically modelled rapid impact compaction, obtaining the following results: RIC with a 9 t hammer falling from 1.1 m in height is useful in silty gravel when improvement at depths of 3 m or less is required. The soil was strongly affected by the method at up to 2 m in depth, where a stiff soil plug formed and the relative density was greater than 100%. The relative density continued to increase at a lower rate up to 4 m in depth.
- The mechanism of RIC was more effective vertically than horizontally and the soil compacted like a column under the anvil. Lateral regions were not strongly influenced by RIC up to 3.5 m from the center. This region was located at 0 to 0.5 m in depth and was assumed to interact with closer compaction points.
- Numerical analysis showed that 54% more blows were needed to reach the final set at 10 to 2 mm; however, the increase in relative density was low at this range. Further blows to reduce the set from 10 mm only resulted in formation of a stiffer soil plug at 0 to 2 m in depth. The soil remained in the medium compaction state at the lower depth of 2 to 3 m and loose compaction at 3 to 4 m. It can be concluded that the optimum set was about 10 mm for the soil considered in the present study. Further numerical analysis is required for other types of soils and compaction patterns.

References

Adam, D., Adam, C., Falkner, F.J. and Paulmichl, I. (2011), "Vibration emission induced by rapid impact compaction", *Proceedings of the 8th International Conference on Structural Dynamics*, *EURODYN*, Leuven, July.

Allen, S. (1996), "The low energy dynamic compaction of soil", Ph.D. Dissertation, University of Wales, Cardiff, UK.

ASTM, (1998), *Annual Book of ASTM Standards: Soils and Rock Division*, West Conshohocken, Philadelphia, PA, USA.

Bathe, K.J. (1996), *Finite Element Procedures*, Englewood Cliffs, New Jersey, USA.

Becker, P.J. (2011), "Assessment of rapid impact compaction for transportation infrastructure applications",

Graduate Thesis, Iowa State University, Ames, IA, USA.
Chow, Y.K., Yang, D.M., Yang, K.Y. and Lee, S.L. (1990), "Monitoring of dynamic compaction by deceleration measurements", *Comput. Geotech.*, **10**(3), 189-209.
Dimaggio, F.L. and Sandler, I.S. (1971), "Material model for granular soils", *Journal of Engineering Mechanics Division, ASCE*, **97**(EM3), 935-950.
Falkner, F.J, Adam, C., Paulmichl, I., Adam, D. and Fürpass, J. (2010), "Rapid impact compaction for middle-deep improvement of the ground-numerical and experimental investigations", *14th Danube-European Conference on Geotechnical Engineering*, Bratislava, Slovakia, June.
Ghassemi, A., Pak, A. and Shahir, H. (2009), "Numerical study of the coupled hydro-mechanical effects in dynamic compaction of saturated granular soils", *Comput. Geotech.*, **37**(1-2), 10-24.
Jia, M. and Zhou, J. (2010), "Investigation of mechanical response induced in dynamic compaction of sandy soils with PFC2D", *GeoShanghai International Conference*, Shanghai, June.
Kristiansen, H. and Davies, M. (2004), "Ground improvement using rapid impact compaction", *13th World Conference on Earthquake Engineering*, Vancouver, Canada, August.
Lee, F.H. and Gu, Q. (2004), "Method for estimating dynamic compaction effect on sand", *Journal of Geotech. Geoenviron. Eng.*, **130**(2), 139-152.
Mayne, P.W. and Jones, J.S. (1983), "Impact stresses during dynamic compaction", *Geotech. Eng.*, **109**(10), 1342-1346.
Merrifield, C.M. and Davies, C.R. (2000), "A study of low-energy dynamic compaction: Field trials and centrifuge modeling", *Geotechnique*, **50**(6), 675-681.
Merrifield, C.M., Cruickshank, M. and Parvizi, M. (1998), "Modelling of low energy dynamic compaction", *Proceedings of Centrifuge 98*, Tokyo, Japan, September.
Oshima, A. and Takada, N. (1997), "Relation between compacted area and ram momentum by heavy tamping", *Proceedings of 14th International Conference on Soil Mechanics and Foundation Engineering*, Hamburg, Germany, September.
Pak, A., Shahir, H. and Ghassemi, A. (2005), "Behavior of dry and saturated soils under impact load during dynamic compaction", *Proceedings of 16th International Conference on Soil Mechanics and Geotechnical Engineering*, Osaka, Japan, September.
Pan, J.L. and Selby, A.R. (2002), "Simulation of dynamic compaction of loose granular soils", *Adv. Eng. Software*, **33**(7-10), 631-640.
Parvizi, M. (1999), "Centrifuge modelling of low energy dynamic compaction", Ph.D. Dissertation. University of Manchester, Manchester, UK.
Parvizi, M. (2006), "Efficiency of dynamic compaction by low energy", *Proceedings 35th Solid Mechanics Conference*, Krakow, Poland, September.
Parvizi, M. (2009), "Soil response to surface impact loads during low energy dynamic compaction", *J. Appl. Sci.*, **9**(11), 2088-2096.
Parvizi, M. and Merrifield, C.M. (2000), "Mechanical behaviour of a sand bed subjected to low energy dynamic compaction modeled in a geotechnical centrifuge", *J. Phys.*, **10**(9), 131-135.
Poran, C.J. and Rodriguez, J.A. (1992), "Finite element analysis of impact behavior of sand", *Soil. Found.*, **32**(4), 68-80.
Rix, G.J., Lai, C.G. and Spang, A.W. (2000), "In situ measurement of damping ratio using surface waves", *J. Geotech. Geoenviron. Eng.*, **126**(5), 472-480.
Roesset, J.M., Kausel, E., Cuellar, V., Monte, J.L. and Valerio, J. (1994), "Impact of weight falling on to the ground", *Geotech. Eng.*, **120**(8), 1394-1412.
Scott, R.A. and Pearce, R.W. (1975), "Soil compaction by impact", *Geotechnique*, **25**(1), 19-30.
Serridge, C.J. and Synac, O. (2006), "Application of the rapid impact compaction (RIC) technique for risk mitigation in problematic soils", *Proceedings of the Conference of the International Association of Engineering Geology*, Nottingham, England, September.
Simpson, L.A., Jang, S.T., Ronan, C.E. and Splitter, L.M. (2008), "Liquefaction potential mitigation using RapidImpact Compaction", *Proceedings of the 4th Conference of Geotechnical Earthquake Engineering and SoilDynamics*, Sacramento, CA, USA, May.

SPI Company (2006), *Report of Geotechnical Investigations for Dynamic Compaction Performed in Assalouyeh, Southern Iran*, Tehran, Iran.

Sun, J.S., Lee, K.H. and Lee, H.P. (2000), "Comparison of implicit and explicit finite element methods for dynamic problems", *J. Mater. Process. Tech.*, **105**(1-2), 110-118.

Tara, D. and Wilson, P. (2004), "Rapid impact compactor ground improvement, vibration monitoring and densification assessment", Report Submitted to Rapid Impact Compactors Ltd., Thurber Engineering Ltd., Delta, BC, Canada.

Vukadin, V. (2013), "The improvement of the loosely deposited sands and silts with the rapid impact compaction technique on Brežice test sites", *Eng. Geol.*, **160**(1)**,** 69-80.

Watts, K.S. and Charles, J.A. (1993), "Initial assessment of a new rapid impact ground compactor", *Proceedings of the Conference on Engineered Fills*, London, UK, September.

Yasrebi, S. and Asghari, E. (2004), "Dynamic compaction in Assalouyeh, Iran", *4th International Conference on Case histories in Geotechnical Engineering*, New York, NY, USA, March.

PL